Journal of Physics: Conference Series **436** (2013) 012084 doi:10.1088/1742-6596/436/1/012084

Interaction of electromagnetic fields and atomic clusters

S Bubin, A G Russakoff and K Varga

Department of Physics and Astronomy, Vanderbilt University, TN-37240, Nashville, USA

E-mail: kalman.varga@vanderbilt.edu

Abstract. In the framework of real-time real-space time-dependent density functional theory complemented with Ehrenfest molecular dynamics we have studied the response of nanostructures to intense femtosecond laser pulses. Examples of applications include laser desorption of hydrogen from graphene and Coulomb explosion of hydrocarbon molecules.

1. Introduction

The basic idea of cluster models is to describe a complex physical system by using a simpler, physically motivated selection of the degrees of freedom. This approach has been successfully used not only in nuclear physics, but in many other areas of research including atomic and molecular physics and quantum chemistry. In nuclear physics, cluster models are used to build basis functions by separating the internal degrees of freedom of groups of nuclei and the wave functions of relative motions between clusters. Using this idea, we have developed a multidomain framework for electronic structure calculations of atomic clusters and nanostructures [1]. In this approach the basis functions of the system are generated from sets of cluster wave functions of groups of atoms. Many other ingredients of this approach, e.g. the use of Taylor time propagators of complex absorbing potentials is familiar and has been developed in nuclear physics as well.

In this contribution, we will present our study of electron and nuclear dynamics induced by strong laser pulses in the framework of the time-dependent density functional theory in real-time and real-space [2, 3, 4, 5, 6, 1]. With the advance of time-dependent probes [7] the investigation of the dynamical behaviour of matter at the nanoscale has become a very important research direction [8, 9, 10, 11, 12, 13, 14, 15, 16]. Comprehensive knowledge of the dynamic behaviour of electrons and ions in condensed-matter systems is pertinent to the development of many modern technologies, such as semiconductor and molecular electronics, optoelectronics, information processing and photovoltaics.

Density functional theory (DFT) is now well established as one of the most efficient methods for computing electronic ground state properties. In its original formulation, DFT only applies to the electronic ground state. Runge and Gross (RG) [17] generalized DFT to time-dependent (TD) systems. According to the RG theorem, for any given initial state of a many-electron system, a TD potential acting on it is uniquely determined by the subsequent time evolution of the one-electron density. Using this theorem, it is possible to formally establish a TD Kohn-Sham (KS) equation from which various one-particle properties of the system can be obtained as functions of time. The resulting theoretical framework is usually referred to as time-dependent density functional theory (TDDFT).

TDDFT has been successfully used in various time-dependent quantum mechanical simulations. The most important applications of the TDDFT approach are (i) non-perturbative calculations with systems in intense laser fields [18, 19, 20], (ii) calculations of optical response, dielectric functions and electronic transitions [21, 22, 23, 24, 25, 26, 27, 28, 29, 30], (iii) calculation of electronic excitations [31, 32, 33], and (iv) time-dependent transport calculations [34, 35, 36].

2. Method

The electron dynamics in our simulations is modelled within real-space real-time TDDFT using the adiabatic local density approximation (ALDA) with the parameterization of Perdew and Zunger [37]. Core electrons are represented by norm-conserving Troullier–Martins pseudopotentials [38]. At the first stage, the initial state of the system is prepared by performing the ground state DFT calculation. Next, the time-dependent Kohn–Sham orbitals, ψ_k, are determined by solving the equation

$$i\hbar\frac{\partial\psi_k(\mathbf{r},t)}{\partial t} = H\psi_k(\mathbf{r},t), \quad k = 1,\ldots,N_{\mathrm{orb}} \tag{1}$$

with the Hamiltonian,

$$H = -\frac{\hbar^2}{2m}\nabla_{\mathbf{r}} + V_{\mathrm{H}}[\rho](\mathbf{r},t) + V_{\mathrm{XC}}[\rho](\mathbf{r},t) + V_{\mathrm{ext}}(\mathbf{r},t), \tag{2}$$

where ρ is the electronic density,

$$\rho(\mathbf{r},t) = 2\sum_{k}^{N_{\mathrm{orb}}} |\psi_k(\mathbf{r},t)|^2, \tag{3}$$

and V_{H} and V_{XC} are the Hartree and exchange-correlation potential, respectively. V_{ext} is the external potential, which includes the potential due to the ions, V_{ions}, and the explicitly time-dependent potential due to the laser electric field. In the dipole approximation, $V_{\mathrm{laser}}(\mathbf{r},t) = \mathbf{r}\cdot\mathbf{E}(t)$. Assuming polarization along the x-axis, the electric field of the laser can be written as

$$\mathbf{E}(t) = \mathbf{e}_x E_{\max}\exp\left[-\frac{(t-\tau)^2}{2a^2}\right]\sin(\omega t). \tag{4}$$

Here parameters a, τ, and $E_{\max}$ define the width, the position of the centre, and the maximum electric field amplitude of the Gaussian envelope respectively, while ω is the frequency of the laser.

The time-propagation of electronic orbitals and density is achieved through the action of the time-evolution operator,

$$U(0,t) = \mathcal{T}\exp\left[-\frac{i}{\hbar}\int H(\mathbf{r},t')dt'\right], \tag{5}$$

where $\mathcal{T}$ denotes time-ordering. In practice, the above expression for $U(0,t)$ is split into a product of multiple time-evolution operators, each corresponding to a short time step Δt,

$$U(0,t) = \prod_q U(t_q, t_q+\Delta t), \quad t_q = q\Delta t, \tag{6}$$

so that the Hamiltonian at time t_q remains nearly commutative with the Hamiltonian at time $t_q + \Delta t$. In all calculations performed in this work we used a time step of 0.72 attoseconds, which we found to provide an acceptable balance of speed, stability, and accuracy for the time-propagation. The actual value of the time step was chosen based on our experience with other hydrocarbons subjected to laser pulses of similar intensity and duration where we monitored the conservation of the total charge[1] and the convergence of the results with decreasing the time

[1] Then the imaginary absorbing potential was switched off. See later.

step. To represent $U(t_q, t_q + \Delta t)$ we employed the fourth order Taylor expansion,

$$\psi_k(\mathbf{r}, t_q + \Delta t) \approx \sum_{n=1}^{4} \frac{1}{n!} \left(-\frac{i\Delta t}{\hbar} H(\mathbf{r}, t_q) \right)^n \psi_k(\mathbf{r}, t_q). \tag{7}$$

In real-space DFT and TDDFT the Kohn–Sham orbitals are represented on discrete points in real space (usually organized in uniform rectangular grids). This brings certain advantages to calculations of sophisticated electron dynamics in the case when a strong laser pulse is applied. The dynamics may involve a significant variation of the electron density within a large volume as well as ionization and fragmentation of the system. It is generally not known in advance how this process occurs. The grid representation of the orbitals allows one to describe an essentially arbitrary time-evolution, as long as the simulation cell (i.e. the area of real space covered by the numerical grids) is sufficiently large. The accuracy of such a representation is easily controlled by a single parameter – the grid spacing. In our calculations we used uniform grids with x-, y-, and z-spacing of 0.25 Å.

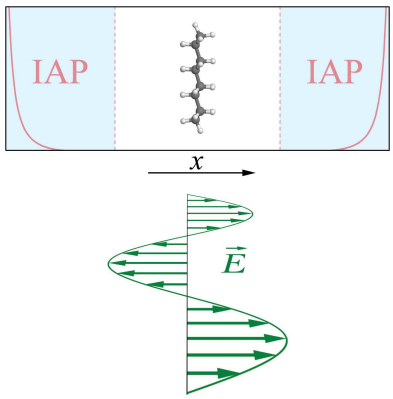

Figure 1. Schematic view of the simulation cell setup: the studied system is in the middle of the box, while the imaginary absorbing potential (IAP) acts on the left- and right-hand side and reaches its maximum at the walls. Laser polarization is along the x-axis.

To allow long time evolution in the calculations with real-space grids it is necessary to negate the effects of zero-boundary conditions, which causes an unphysical reflection of the wave function from the walls of the simulation cell. Given typical electron velocities and a length of the simulation cell that exceeds the system size by 5-10 Å in all directions, it only takes a few femtoseconds for the electrons to reach the boundaries. This problem is traditionally solved by using an imaginary absorbing potential (IAP) or a real mask-function (a concept closely related to IAP). In our calculations we employed an imaginary absorbing potential in the form proposed by Manolopoulos [39] with an additional softening parameter to suppress extremely large IAP magnitudes at the boundaries, which can cause numerical instabilities in grid-type approaches. Since the momentum of the electrons escaping from the system lies primarily in the x-direction, the IAP in our calculations was chosen such that it only had nonzero value in the region of space next to the x-boundaries. A schematic of this set up is shown in Fig. 1.

In the middle of the simulation cell, which contains the studied system, the IAP is zero by definition and does not influence the system in any way. While the ponderomotive amplitude for some of the laser intensities used in our calculations well exceeded the length of the IAP-free region, our previous experience with calculations having a similar computational setup and comparable laser pulses showed that one does not need to have an extremely large simulation cell to obtain converged results.

The ionic motion in this work is simulated by means of the Ehrenfest approach [40], in which the forces on ions are computed as the derivatives of the expectation value of the total electronic energy with respect to ionic positions, i.e.

$$M_i \frac{d^2\mathbf{R}_i}{dt^2} = \sum_{j \neq i}^{N_{\text{ions}}} \frac{Z_i Z_j (\mathbf{R}_i - \mathbf{R}_j)}{|\mathbf{R}_i - \mathbf{R}_j|^3} - \nabla_{\mathbf{R}_i} \int V_{\text{ion}}(\mathbf{r}, \{\mathbf{R}\}) \rho(\mathbf{r}, t) d\mathbf{r}. \tag{8}$$

In the above classical equation of motion M_i is the mass of the ith ion and Z_i is its valence charge (the charge of the atom minus the charge of the core used in the pseudopotential). The set of equations (8) for $i = 1 \dots N_{\text{ions}}$ is integrated simultaneously with the set of time-dependent Kohn-Sham equations (1), although the integration time step for (8) may be chosen to be somewhat longer. To integrate equation (8) the well known Verlet algorithm is used.

3. Applications

In this section we present a few selected applications of the computational approach.

3.1. Graphene and graphane fragments in high-intensity laser pulses

An understanding of the interaction of intense, ultrashort laser pulses and graphene is a key prerequisite for both laser patterning and cleaning, as well as for applications of graphene in optical devices. Laser-induced bond breaking, defect formation, and damage mechanisms have been intensively investigated since the advent of high power laser pulses [41, 42]. Unlike their long-pulse counterparts, material processing with ultrashort-pulse lasers have negligible heat diffusion effects, minimal plasma absorption, and require smaller laser fluences for processing, making them ideal for achieving high spatial resolution [43, 44]. The effect of the laser pulse on the material strongly depends on the absorbed energy, which is determined by the material properties, as well as on the strength, intensity, shape, and duration of the pulse.

A general illustration of the hydrogen desorption process in a graphane fragment is given in Fig. 2. As the oscillation of the electric field grows, the amplitude of the electron density oscillations grows as well. Eventually, when it becomes large enough, the hydrogen ions on both sides of the surface start moving away (at that moment the entire system is heavily ionized). It is interesting to note that at the initial stage of the motion, when the hydrogen ions are still close (1-4 Å) to the carbon ions they were initially attached to, the charge density around the H ions changes dramatically depending on the instantaneous direction of the electric field. Essentially, the state of the hydrogen ions oscillates between a bare proton and a hydrogen atom. These oscillations decay as the hydrogen ions move away from the surface. With each oscillation the laser continues to ionize the main target. Bare protons in close proximity (a few Å) to the main target, can recapture a small fraction of the escaped electrons.

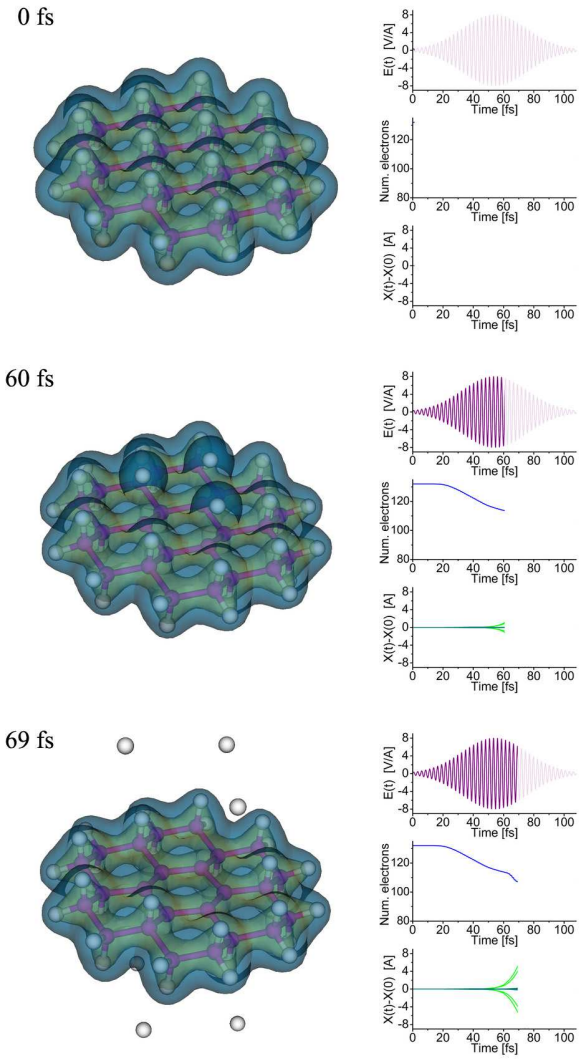

Figure 2. Time-evolution of the electron density and ionic positions in graphane fragment subjected to a 790nm, 35.4 fs laser pulse with the maximum electric field amplitude of 8 V/Å (enhanced online).

However, when the direction of the electric field gets reversed, those electrons will not stay with the protons. At the time when the laser pulse is near its end the hydrogen ions are sufficiently far from the carbon surface and carry practically no electron charge with them.

Comparing graphene and graphane, the calculations show that graphene exhibits a considerably higher immediate damage threshold due to its strictly planar structure. Finite temperature simulations that distort the planar symmetry yield structural damage at lower intensities. The survival of irradiated graphene for a time that significantly exceeds tens of femtoseconds (after the pulse) is likely to depend on experimental conditions such as laser spot size and the presence of a substrate which determines its ability to quickly gain electrons from the bulk of the material to replace those lost during the laser pulse. The results obtained in the simulations of graphane demonstrate that by choosing the proper laser wavelength and intensity it is possible to achieve a desorption of hydrogen atoms without destroying the underlying layer of carbon atoms. Such a selective desorption achieved by tuning the two parameters is, in fact, a very basic realization of Quantum Optimal Control – a framework that is aimed to actively manipulate quantum dynamics using external time-dependent fields [45, 46, 47, 48, 49].

3.2. Coulomb explosion of hydrocarbon molecules

The strong-field ionization and fragmentation of hydrocarbon molecules is a prototypical example of the Coulomb explosion of polyatomic molecules, and it has been the subject of several experiments [50, 51, 52, 53, 54, 55]. An important quantity measured in these experiments is the kinetic energy distribution of the protons ejected during the fragmentation.

We have investigated the Coulomb explosion of methane, CH_4, and 1,3-butadiene, C_4H_6, in the framework of the time-dependent density functional theory and compared the results of the simulations to experimental data.

The dynamics of the ions, i.e. the displacements from their initial positions, $|\mathbf{R}_j(t) - \mathbf{R}_j(0)|$, and the evolution of kinetic energies, are illustrated in Figs. 3.2(c)-(f). As can be seen, the

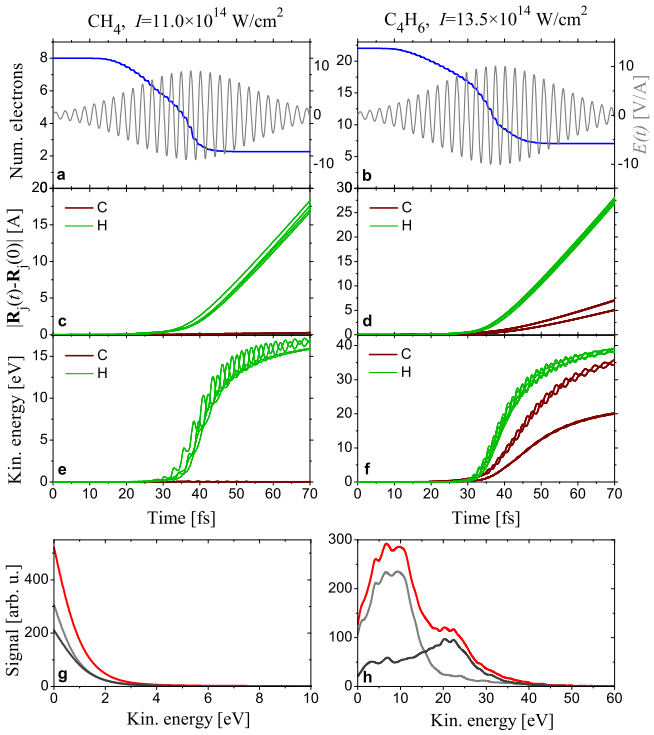

Figure 3. (a, b) Number of valence electrons remaining in the molecular system (blue lines) during ionization by a laser pulse (gray lines) for methane and 1,3-butadiene. (c, d) Displacements of individual protons (green lines) and carbon ions (dark red lines) from their initial positions. (e, f) Kinetic energies of individual protons (green lines) and carbon ions (dark red lines). While the data shown for the displacements and kinetic energies is for some randomly picked molecular spatial orientation, the same qualitative behaviour could be observed for the majority of other orientations. (g, h) Measured carbon energy spectrum (red line) decomposed into the contributions of singly and doubly charged carbons (gray lines).

molecules fragment completely and all protons get ejected simultaneously in a concerted process. The protons fly out in different directions as governed by the conservation of the total momentum but have very similar kinetic energies, see Figs. 3.2(e) and (f). The fact that the protons are ejected concertedly is also reflected by the near zero kinetic energy of the remaining carbon ion of CH_4 in both the simulated, Fig. 3.2(e), and measured data, Fig. 3.2(g). The measured carbon energy spectrum can be decomposed into the contributions of singly and doubly charged carbons (see the gray lines). Both of them peak at zero kinetic energy in accordance with a concerted, all-at-once emission of protons, which leaves the central carbon ion at rest. The similarity of the final kinetic energies of all ejected protons is most pronounced in the simulations with the highest laser intensity performed for the C_4H_6 molecule, Figs. 3.2(d) and (f). After the simultaneous departure of the protons the heavy carbon skeletal structure separates in two steps, with each of them involving the explosion of two carbon ions, leading to two distinctly different final carbon energies. These dynamics are nicely reflected in the measured bimodal carbon energy spectrum in Fig. 3.2(h) with peaks at approx. 8 and 22 eV. A decomposition of the measured spectrum into the contributions of the singly and doubly charged carbon ions, shown by gray lines, reveals that the two peaks in the spectrum are caused by doubly and singly charged carbon ions, respectively. Fig. 3.2(e) shows that for the slightly weaker laser peak intensity of 11.0×10^{14} W/cm^2 used for the CH_4 molecule, the high similarity of the proton energies observed for the high-intensity case of the 1,3-butadiene simulation becomes less pronounced. In the second simulation for CH_4 with the still smaller intensity of 6.7×10^{14} W/cm^2, the difference in the individual proton kinetic energies was quite noticeable and for some of the initial spatial orientations the molecule did not undergo a complete fragmentation during the simulation time.

3.3. Fragmentation of Uracil in Collisions with Neutral Potassium

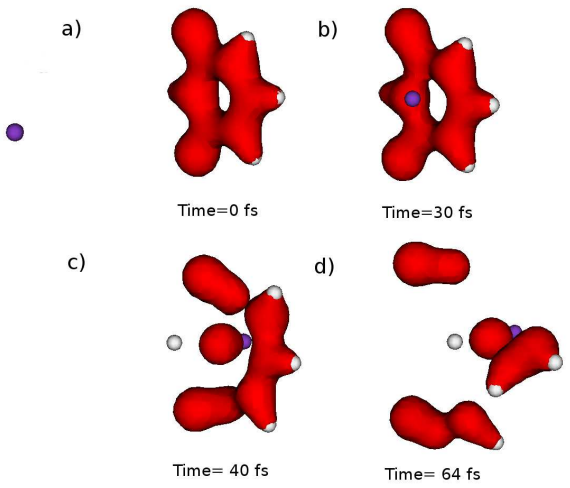

Figure 4. Time-evolution of the electron density and ionic positions of uracil during collision with a potassium atom with kinetic energy 200 eV, and initial separation of 10 Å.

An understanding of the interaction of moving particles with biological systems, RNA and DNA in particular, is an important prequisite for discerning the effects of radiation damage and for developing more efficient radiation therapies [56]. A complete description of the effects of particle collisions in DNA and RNA requires knowledge of both the direct damage from the particle, and the indirect damage caused by secondary particles, including low energy electrons ejected through ionization and particles ejected through molecular fragmentation [57]. Collisions involving neutral potassium are of particular interest since recent experimental work has shown that selective bond scission may be achieved by tuning the potassium atom's kinetic energy [58].

Figure 4 shows a simulation, within the framework of time dependent density functional theory, of the collision of a neutral potassium atom with the RNA nucleobase uracil, $C_4H_4N_2O_2$. The potassium atom's initial kinetic energy is 200 eV, and is separated from the uracil molecule by 10 Å. The total run time for the simulation is 64 fs. Prior to collision we see significant distortion of the uracil's structure, and subsequent fragmentation as the potassium atom passes through the uracil molecule.

Future work will include varying the potassium atom's kinetic energy and impact parameter, varying the orientation of the molecule, and a study of collisions with other nucleobases. Observables to be probed include the energy and charge transferred from the potassium to the molecule.

4. Summary

With the advent of powerful light sources [59, 60], the study of the interaction of strong short laser pulses with matter has become a centre of intense research interest. In this work, we have carried out first-principles time-dependent simulations of the interaction of intense short laser pulses with nanostructures using time-dependent density functional calculations complemented with Ehrenfest molecular dynamics. These first principles simulations are indispensable tools to gain insight into the physical mechanisms behind highly nonequilibrium and nonlinear processes, such as laser-induced structural deformation and Coulomb explosion. The presented TDDFT framework is a low-cost and high-accuracy approach that can be used to simulate the electron and nuclear dynamics in strong external fields, to explain experimental results and to design new experiments. Computational approaches developed in nuclear cluster theory have been utilized in this work, and with the continuous growth in computional power we expect that this cross fertilization can further advance other research fields as well.

References

[1] Goncharov V A and Varga K 2011 *Phys. Rev. B* **83** 035118
[2] Bubin S and Varga K 2012 *Phys. Rev. B* **85**(20) 205441
[3] Bubin S and Varga K 2011 *Appl. Phys. Lett.* **98** 154101
[4] Bubin S and Varga K 2011 *J. Appl. Phys.* **110** 064905
[5] Bubin S, Wang B, Pantelides S and Varga K 2012 *Phys. Rev. B* **85**(23) 235435
[6] Driscoll J A, Bubin S and Varga K 2011 *Phys. Rev. B* **83** 233405
[7] Krausz F and Ivanov M 2009 *Rev. Mod. Phys.* **81** 163–234
[8] Kruger M, Schenk M and Hommelhoff P 2011 *Nature* **475** 78–81 ISSN 0028-0836 URL `http://dx.doi.org/10.1038/nature10196`
[9] Fohlisch A, Feulner P, Hennies F, Fink A, Menzel D, Sanchez-Portal D, Echenique P M and Wurth W 2005 *Nature* **436** 373–376 ISSN 0028-0836 URL `http://dx.doi.org/10.1038/nature03833`
[10] Hamoudi H, Neppl S, Kao P, Schüpbach B, Feulner P, Terfort A, Allara D and Zharnikov M 2011 *Phys. Rev. Lett.* **107** 027801
[11] Young L, Kanter E P, Krassig B, Li Y, March A M, Pratt S T, Santra R, Southworth S H, Rohringer N, DiMauro L F, Doumy G, Roedig C A, Berrah N, Fang L, Hoener M, Bucksbaum P H, Cryan J P, Ghimire S, Glownia J M, Reis D A, Bozek J D, Bostedt C and Messerschmidt M 2010 *Nature* **466** 56–61 ISSN 0028-0836 URL `http://dx.doi.org/10.1038/nature09177`
[12] Ikeura-Sekiguchi H and Sekiguchi T 2007 *Phys. Rev. Lett.* **99** 228102
[13] Cavalieri A L, Muller N, Uphues T, Yakovlev V S, Baltuska A, Horvath B, Schmidt B, Blumel L, Holzwarth R, Hendel S, Drescher M, Kleineberg U, Echenique P M, Kienberger R, Krausz F and Heinzmann U 2007 *Nature* **449** 1029–1032 ISSN 0028-0836 URL `http://dx.doi.org/10.1038/nature06229`
[14] Haessler S, Caillat J, Boutu W, Giovanetti-Teixeira C, Ruchon T, Auguste T, Diveki Z, Breger P, Maquet A, Carre B, Taieb R and Salieres P 2010 *Nat Phys* **6** 200–206 ISSN 1745-2473 URL `http://dx.doi.org/10.1038/nphys1511`
[15] Nordlund D, Ogasawara H, Bluhm H, Takahashi O, Odelius M, Nagasono M, Pettersson L G M and Nilsson A 2007 *Phys. Rev. Lett.* **99** 217406
[16] Muino R D, Snchez-Portal D, Silkin V M, Chulkov E V and Echenique P M 2011 *Proceedings of the National Academy of Sciences* **108** 971–976 (*Preprint* `http://www.pnas.org/content/108/3/971.full.pdf+html`) URL `http://www.pnas.org/content/108/3/971.abstract`
[17] Runge E and Gross E K U 1984 *Phys. Rev. Lett.* **52** 997
[18] Yabana K and Bertsch G F 1996 *Phys. Rev. B* **54** 4484–4487
[19] Chu X and Chu S I 2001 *Phys. Rev. A* **64** 063404
[20] Kawashita Y, Nakatsukasa T and Yabana K 2009 *J. Phys. Condens. Matter* **21** 064222
[21] Iwata J I, Yabana K and Bertsch G F 2001 *J. Chem. Phys.* **115** 8773–8783
[22] Nakatsukasa T and Yabana K 2001 *J. Chem. Phys.* **114** 2550–2561

[23] Stott M J and Zaremba E 1980 *Phys. Rev. A* **21** 12–23
[24] Tsolakidis A, Sánchez-Portal D and Martin R M 2002 *Phys. Rev. B* **66** 235416
[25] Kootstra F, de Boeij P L and Snijders J G 2000 *J. Chem. Phys.* **112** 6517–6531
[26] Bertsch G F, Iwata J I, Rubio A and Yabana K 2000 *Phys. Rev. B* **62** 7998–8002
[27] van Gisbergen S J A, Snijders J G and Baerends E J 1998 *J. Chem. Phys.* **109** 10657–10668
[28] Frediani L, Rinkevicius Z and Ågren H 2005 *J. Chem. Phys.* **122** 244104
[29] Takimoto Y, Vila F D and Rehr J J 2007 *J. Chem. Phys.* **127** 154114
[30] Yabana K and Bertsch G F 1999 *Phys. Rev. A* **60** 1271–1279
[31] Görling A 1996 *Phys. Rev. A* **54** 3912–3915
[32] Doltsinis N L and Sprik M 2000 *Chem. Phys. Lett.* **330** 563 – 569
[33] Adamo C, Scuseria G E and Barone V 1999 *J. Chem. Phys.* **111** 2889–2899
[34] Kurth S, Stefanucci G, Almbladh C O, Rubio A and Gross E K U 2005 *Phys. Rev. B* **72** 035308
[35] Qian X, Li J, Lin X and Yip S 2006 *Phys. Rev. B* **73** 035408
[36] Marini A, Del Sole R and Rubio A 2003 *Phys. Rev. Lett.* **91** 256402
[37] Perdew J P and Zunger A 1981 *Phys. Rev. B* **23** 5048–5079
[38] Troullier N and Martins J L 1991 *Phys. Rev. B* **43** 1993–2006
[39] Manolopoulos D E 2002 *J. Chem. Phys.* **117** 9552
[40] Ehrenfest P 1927 *Z. Phys.* **45**(7) 455–457
[41] Carr C W, Radousky H B, Rubenchik A M, Feit M D and Demos S G 2004 *Phys. Rev. Lett.* **92**(8) 087401
[42] Lenzner M, Krüger J, Sartania S, Cheng Z, Spielmann C, Mourou G, Kautek W and Krausz F 1998 *Phys. Rev. Lett.* **80**(18) 4076–4079
[43] Fan C H and Longtin J P 2001 *Appl. Opt.* **40** 3124–3131
[44] Yao Y L, Chen H and Zhang W 2005 *Int. J. Adv. Manuf. Technol.* **26**(5) 598–608
[45] Assion A, Baumert T, Bergt M, Brixner T, Kiefer B, Seyfried V, Strehle M and Gerber G 1998 *Science* **282** 919–922
[46] Shapiro M and Brumer P 2003 *Principles of Quantum Control of Molecular Processes* (New York: Wiley)
[47] Werschnik J and Gross E K U 2007 *J. Phys. B* **40** R175
[48] Brif C, Chakrabarti R and Rabitz H 2010 *New J. Phys.* **12** 075008
[49] Krieger K, Castro A and Gross E K U 2011 *Chem. Phys.* **391** 50 – 61
[50] Cornaggia C, Normand D and Morellec J 1992 *J. Phys. B* **25** L415–L422
[51] Cornaggia C, Schmidt M and Normand D 1995 *Phys. Rev. A* **51** 1431–1437
[52] Markevitch A N, Romanov D A, Smith S M and Levis R J 2004 *Phys. Rev. Lett.* **92** 063001
[53] Shimizu S, Kou J, Kawato S, Shimizu K, Sakabe S and Nakashima N 2000 *Chem. Phys. Lett.* **317** 609–614
[54] Palaniyappan S, Mitchell R, Ekanayake N, Watts A, White S, Sauer R, Howard L, Videtto M, Mancuso C, Wells S, Stanev T, Wen B, Decamp M and Walker B 2010 *Phys. Rev. A* **82** 043433
[55] Roither S, Xie X, Kartashov D, Zhang L, Schöffler M, Xu H, Iwasaki A, Okino T, Yamanouchi K, Baltuska A and Kitzler M 2011 *Phys. Rev. Lett.* **106**(16) 163001
[56] Schulz-Ertner D, Nikoghosyan A, Thilmann C, Haberer T, Jkel O, Karger C, Kraft G, Wannenmacher M and Debus J 2004 *International Journal of Radiation Oncology*Biology*Physics* **58** 631 – 640 ISSN 0360-3016
[57] de Vries J, Hoekstra R, Morgenstern R and Schlathölter T 2003 *Phys. Rev. Lett.* **91**(5) 053401
[58] Almeida D, Ferreira da Silva F, Garcia G and Limão Vieira P 2013 *Phys. Rev. Lett.* **110**(2) 023201
[59] Protopapas M, Keitel C H and Knight P L 1997 *Rep. Prog. Phys.* **60** 389
[60] Mourou G A, Barry C P J and Perry M D 1998 *Phys. Today* **51** 22–28